DDS-LTP

Neural Network algorithms for
magnetic diagnostics in the LTP

Ref.	S2-IEC-TN-3052
Version	1.0
Date	11-Mar-2009
Page	1/20

Neural Network algorithms for magnetic diagnostics in the LTP

Doc. Ref.: **S2-IEC-TN-3052**   Issue: **1.0**   Date: **11-Mar-2009**
CI number: **L 32D0**

Approval List

	NAME	SIGNATURE	DATE
Prepared by:	M. Diaz-Aguiló E. García-Berro A. Lobo		11-March-2009
Revised by:	A. Lobo		11-March-2009
Approved by:	A. Lobo		11-March-2009
Authorised by:	I. Lloro		11-March-2009

DDS-LTP

Neural Network algorithms for
magnetic diagnostics in the LTP

Ref.	S2-IEC-TN-3052
Version	1.0
Date	11-Mar-2009
Page	2/20

(Intentionally blank)

DDS-LTP

Neural Network algorithms for
magnetic diagnostics in the LTP

Ref.	S2-IEC-TN-3052
Version	1.0
Date	11-Mar-2009
Page	2/20

	DDS-LTP	**Ref.**	S2-IEC-TN-3052
IEEC	Neural Network algorithms for	**Version**	1.0
	magnetic diagnostics in the LTP	**Date**	11-Mar-2009
		Page	3/20

Document Distribution List

Name	Position	Company
Ivan Lloro		IEEC
Stefano Vitale		University of Trento
Karsten Danzmann		AEI Hannover
Paul McNamara		*ESA*
Laurent Trougnou	EMC and Magnetics Engineer	*ESA*
Bengt Johlander	Senior Instrument System Engineer	*ESA*
César García	*LPF* Payload Manager	*ESA*

	DDS-LTP	**Ref.**	S2-IEC-TN-3052
IEEC		**Version**	1.0
	Neural Network algorithms for	**Date**	11-Mar-2009
	magnetic diagnostics in the LTP	**Page**	4/20

Document Status Sheet

Author	Issue	Date	Page(s)	Change description
M DiazAguilo	1.0	11/03/2009	All	First version

Table of Contents

List of Figures

List of Tables

Acronyms

AEI Albert-Einstein-Institut, Max-Planck-Institut fr Gravitationsphysik
ASU Astrium Ltd., Astrium UK
CI Configuration Item
DC Direct Current
DDS Data Management and Diagnostics Sub-System

DMU	Data Management Unit
ESA	European Space Agency
ICL	Imperial College of London
IEEC	Institut d'Estudis Espacials de Catalunya
IFAE	Institut de Física d'Altes Energies (Barcelona, Spain)
LCA	LTP Core Assembly
LISA	Laser Interferometer Space Antenna
LPF	LISA Pathfinder (formerly SMART-2)
LTP	LISA Technology Package
LTPA	LTP Architect
NASA	National Aeronautics and Space Administration
NTE	Nuevas Tecnologías Espaciales, S.A. (Lliçà d'Amunt, Spain)
PDF	Probability Density Function
TM	Telemetry / Test mass

Applicable documents

Ref.	Title	Doc Number	Issue	Date
AD1	Science Requirements and Top-level Architecture Definition for the LISA Technology Package (LTP) on Board LISA Pathfinder (SMART-2)	LTPA-UTN-ScRD	3.1	30-06-2005

Reference documents

Ref.	Title	Doc Number	Issue	Date
RD1	LTP Magnetic Field Interpolation	S2-IEC-OTH-3026	1.0	25-11-2008
RD2	Vojislav Kecman, *Learning and soft computing*	The MIT Press	1st edition	2001

IEEC

DDS-LTP

Neural Network algorithms for
magnetic diagnostics in the LTP

Ref.	S2-IEC-TN-3052
Version	1.0
Date	11-Mar-2009
Page	8/20

1 Introduction and scope of this document

The Magnetic Diagnostics Subsystem of the LTP includes a set of four tri-axial fluxgate magnetometers, intended to sense with high precision the magnetic field at the positions they occupy in the LCA. Their readouts do not however provide a direct measurement of the magnetic field at the TMs, and an interpolation method must be implemented to obtain that information. However, such interpolation process faces serious difficulties: indeed, the size of the interpolation region, i.e., the LCA interior, is excessive for a *linear* interpolation to be reliable, but the number of magnetometer channels does not provide sufficient data to go beyond that (poor) approximation.

This document sketches what could be a possible alternative to address the magnetic interpolation problem by means of *neural network* algorithms, and gives a few examples. At present, results look promising, hence the method is under exploration for improvement. The key point in this proposal is the ability neural networks have to *learn* from suitable *training* feedback. It appears that learning efficiency can be best improved by making use of data obtained in on-ground measurements prior to mission launch in all relevant satellite locations and real operation conditions.

2 Detailed description of the problem

Magnetic noise in the LTP is budgetted to be a significant fraction of the total readout noise: $1.2 \times 10^{-14}\,\mathrm{m\,s^{-2}\,Hz^{-1/2}}$ out of $3 \times 10^{-14}\,\mathrm{m\,s^{-2}\,Hz^{-1/2}}$ —see Table 8.1 in [AD1]. This noise occurs because residual magnetisation and susceptibility in the proof masses couple to the surrounding magnetic field, giving rise to a force

$$\mathbf{F} = \left\langle \left[\left(\mathbf{M} + \frac{\chi}{\mu_0}\mathbf{B} \right) \cdot \boldsymbol{\nabla} \right] \mathbf{B} \right\rangle V \qquad (2.1)$$

in each of the TMs, where

$\mathbf{B}$	Magnetic field in the TM
$\mathbf{M}$	Density of magnetic moment (*magnetisation*) of the TM
V	Volume of the TM
χ	Magnetic susceptibility of the TM
μ_0	Vacuum magnetic constant ($4\pi \times 10^{-7}\,\mathrm{m\,kg\,s^{-2}\,A^{-2}}$)
$\langle \cdots \rangle$	TM volume avergage of enclosed quantity

Magnetic noise is generated because the magnetic field and its gradient randomly fluctuate in the regions occupied by the TMs[1]. Quantitative assessment of magnetic noise in the LTP therefore requires real-time monitoring of the magnetic field, which in LPF is done by means of a set of four tri-axial fluxgate magnetometers. These devices have a high permeability magnetic core, which drives a design constraint to keep them somewhat far from the TMs. The price of

---

[1] Additional noise comes from TM susceptibility and magnetic remanence fluctuations, normally expected to be much less important.
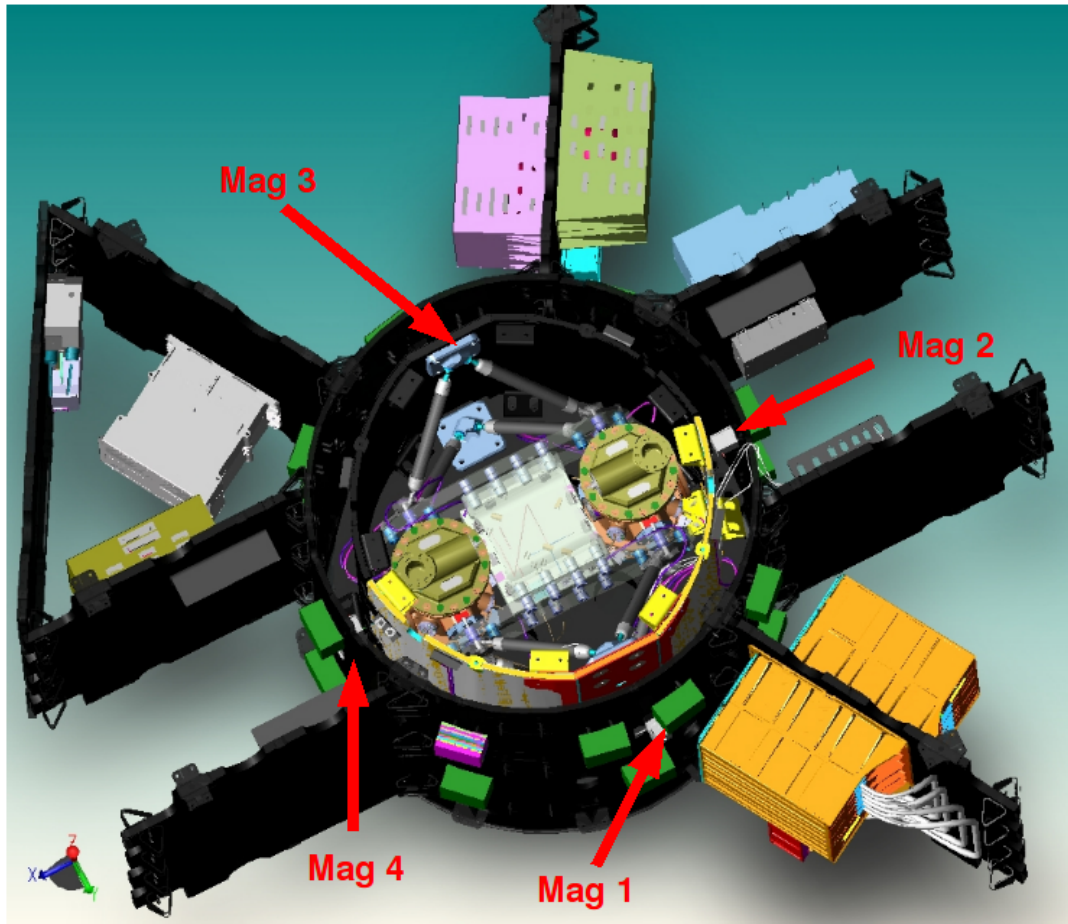
Figure 2.1: Schematic of the LPF Science-craft: The LCA is in the centre, surrounded by a double cylindrical shield, and outside it a number of electronic boxes are represented; most of them are sources of magnetic field. The four magnetometers are the white little boxes indicated by the arrows, and are mounted across the two cylindrical shells.

that is of course that an interpolation problem needs to be solved before the field in the TMs can be inferred.

The sources of magnetic field are essentially due to components inside the spacecraft (S/C), as the interplanetary magnetic field is orders of magnitude weaker. There are no sources of magnetic field inside the LTP Core Assembly (LCA), all being placed within the S/C, outside the LCA walls —see figure 2.1. The number of identified sources is in the order of 50, and they can be modelled as magnetic dipoles in first approximation. Refinements may be useful, but this is not an issue for this document.

What matters instead is that, the sources being *outside* the LCA, the magnetic field is smaller towards the centre of the LCA than it is in its periphery, where the magnetometers take measurements. Figure 2.2 shows a qualitative diagram of the situation.

As we shall now see, there is no interpolation method which can give account of this circumstance on the basis of the information produced by the three vector magnetometers.
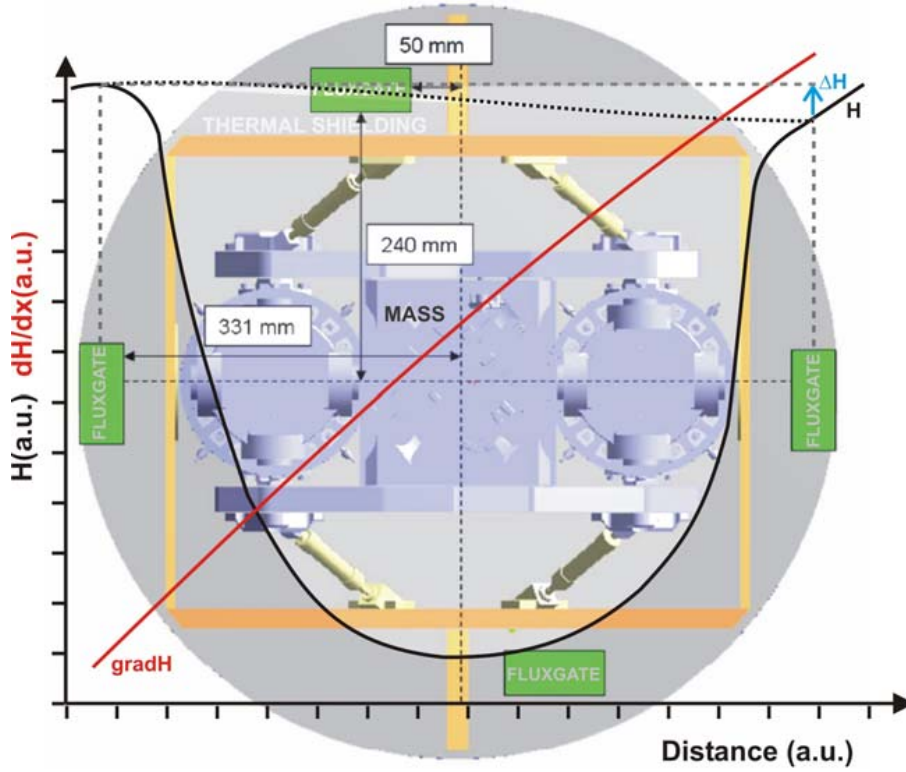
Figure 2.2: Qualitative behaviour of the magnetic field and gradient inside the LCA. Scales are not real.

2.1 Interpolation theory

We will treat the LCA region as a vacuum. This is a quite reasonably accurate hypothesis, as the materials inside it are essentially non-magnetic. Accordingly, the magnetic field has zero divergence and rotational[2]:

$$\boldsymbol{\nabla}\!\cdot\!\mathbf{B}(\mathbf{x},t) = 0 \quad \text{and} \quad \boldsymbol{\nabla} \times \mathbf{B}(\mathbf{x},t) = 0 \tag{2.2}$$

We thus have

$$\boldsymbol{\nabla} \times \mathbf{B}(\mathbf{x},t) = 0 \quad \Rightarrow \quad \mathbf{B}(\mathbf{x},t) = \boldsymbol{\nabla}\Psi(\mathbf{x},t) \tag{2.3}$$

where $\Psi(\mathbf{x},t)$ is a scalar function. Because $\boldsymbol{\nabla}\!\cdot\!\mathbf{B}(\mathbf{x},t) = 0$, too, it immediately follows that $\Psi(\mathbf{x},t)$ is a harmonic function, or

$$\nabla^2\Psi(\mathbf{x},t) = 0 \tag{2.4}$$

The solution to this equation can be expressed as an orthogonal series of the form

$$\Psi(\mathbf{x},t) = \sum_{l=0}^{\infty} \sum_{m=-l}^{l} M_{lm}(t)\, r^l\, Y_{lm}(\mathbf{n}) \tag{2.5}$$

where

$$r \equiv |\mathbf{x}|\,, \qquad \mathbf{n} \equiv \mathbf{x}/r \tag{2.6}$$

---

[2] Given the distances in the spacecraft, in the order of one metre, propagation effects will be neglected. Time dependence will therefore be purely parametric, i.e., the time variable will just label the value the field takes on at that time.

	DDS-LTP	Ref.	S2-IEC-TN-3052
IEEC		Version	1.0
	Neural Network algorithms for	Date	11-Mar-2009
	magnetic diagnostics in the LTP	Page	11/20

are the spherical coordinates of the field point $\mathbf{x}$, whose origin is by (arbitrary) convention assumed in the geometric centre of the LCA. In equation (2.5), the terms in r^{-l-1} have been dropped out of the series, since the field cannot diverge at the centre of the LCA. Actually, the expansion (2.5) is only valid in a region interior to the closest field source. Finally, the coefficients $M_{lm}(t)$, which will be called *multipole coefficients* in the sequel, depend on the sources of magnetic field, and boundary conditions.

To obtain the field components we go back to equation (2.3):

$$\mathbf{B}(\mathbf{x}, t) = \boldsymbol{\nabla}\Psi(\mathbf{x}, t) = \sum_{l=0}^{\infty} \sum_{m=-l}^{l} M_{lm}(t)\, \boldsymbol{\nabla}[r^l\, Y_{lm}(\mathbf{n})] \tag{2.7}$$

In terms of the above development, the question we need to address is: how many terms of the series can we possibly determine on the basis of the information available, i.e., that provided by the magnetometers? Or, in other words, how many multipole coefficients can be calculated on the basis of the magnetometers readout data? Then, finally, to which accuracy can we estimate the actual magnetic field after the maximum number of multipole coefficients have been calculated?

The answer to the first two questions above is actually quite simple. The number of magnetometer data channels is 12: three channels per magnetometer, as the devices are tri-axial. The approximate magnetic field is given by cutting off the series in equation (2.7) to include terms up to a maximum value of $l = l_{\max} \equiv L$, or

$$\mathbf{B}_{\mathrm{estim}}(\mathbf{x}, t) = \sum_{l=1}^{L} \sum_{m=-l}^{l} M_{lm}(t)\, \boldsymbol{\nabla}[r^l\, Y_{lm}(\mathbf{n})] \tag{2.8}$$

The number of terms in this sum is

$$N(L) = \sum_{l=1}^{L} (2l + 1) = L(L + 2) \tag{2.9}$$

since the monopole ($l = 0$) does not contribute. We thus have $N(2) = 8$, while $N(3) = 15$. This means that that we cannot pursue the series beyond the quadrupole($l = 2$) terms: indeed, we only have 12 data channels, so have some redundancy to determine $M_{lm}(t)$ up to $l = 2$, but lack information to evaluate the next seven octupole terms[3].

In order to make a best estimate of the $M_{lm}(t)$, a least square criterion is set up as follows: we define the quadratic error as

$$\varepsilon^2(M_{lm}) = \sum_{s=1}^{4} |\mathbf{B}_{\mathrm{measured}}(\mathbf{x}_s, t) - \mathbf{B}_{\mathrm{estim}}(\mathbf{x}_s, t)|^2 \tag{2.10}$$

where the sum extends over the number of magnetometers, situated at positions $\mathbf{x}_s$ ($s = 1,\ldots,4$), and then find those values of M_{lm} which minimise that error, i.e.,

$$\frac{\partial \varepsilon^2}{\partial M_{lm}} = 0 \tag{2.11}$$

---

[3] A clarification is in order here. The multipole coefficients $M_{lm}(t)$ are actually *complex* numbers, which may mislead one into inferring that actually *fewer* can be calculated. This is however not so beacuse of the symmetry $M_{lm}(t) = (-1)^m M_{l,-m}^*(t)$, which ensures $\mathbf{B}(\mathbf{x}, t)$ is actually a real number.

	DDS-LTP	**Ref.**	S2-IEC-TN-3052
IEEC	**Neural Network algorithms for**	**Version**	1.0
	magnetic diagnostics in the LTP	**Date**	11-Mar-2009
		Page	12/20

Once this system of equations is solved, the estimated coefficients M_{lm} are replaced into equation (2.8) and then the spatial arguments $\mathbf{x}$ are substituted by the positions $\mathbf{x}_s$ of each test mass, respectively, to finally obtain the sought field interpolations. This process needs to be repeated for each instant t of time at which measurements are taken, thereby generating the magnetic field time series. The gradient is also recovered by taking the derivatives of equation (2.8):

$$\left.\frac{\partial B_i}{\partial x_j}\right|_{\text{estim}}(\mathbf{x},t) = \sum_{lm} M_{lm}(t)\,\frac{\partial^2}{\partial x_i\,\partial x_j}\left[r^l\,Y_{lm}(\mathbf{n})\right] \tag{2.12}$$

which obviously verify the constraints (2.2).

2.2 Discussion so far

As just seen, our multipole expansion must end in $L=2$. Explicitly,

$$\mathbf{B}_{\text{estim}}(\mathbf{x},t) = \sum_{l=1}^{2}\sum_{m=-l}^{l} M_{lm}(t)\,\boldsymbol{\nabla}[r^l\,Y_{lm}(\mathbf{n})] \tag{2.13a}$$

$$\left.\frac{\partial B_i}{\partial x_j}\right|_{\text{estim}}(\mathbf{x},t) = \sum_{l=1}^{2}\sum_{m=-l}^{l} M_{lm}(t)\,\frac{\partial^2}{\partial x_i\,\partial x_j}\left[r^l\,Y_{lm}(\mathbf{n})\right] \tag{2.13b}$$

We now recall that $r^l\,Y_{lm}(\mathbf{n})$ is a polynomial of degree l in $\mathbf{x}$, e.g.,

$$r^2\,Y_{20}(\mathbf{n}) = \sqrt{\frac{5}{16\pi}}\left(2z^2 - x^2 - y^2\right)\,, \quad \text{etc.} \tag{2.14}$$

so that in pratice equation (2.13a) is only a *linear* interpolation of the field between the values it has in four peripheral points, where the magnetometers are, and the interior region, where the proof masses are[4]. There is therefore little hope that a trend in the field values, such as qualitatively represented in figure 2.2, be reproduced with this approximation. At least a *quadratic* term would be required, but that would need a multipole expansion up to $L=3$, which in turn would only be possible if a fifth magnetometer readout were available: in this case we would have 15 sensor channels, just enough to determine the M_{lm} up to octupole order.

Likewise, the gradient fo the field, equation (2.13b) is just constant, again a very poor approximation to the reality of facts.

The bottomline of this failure is that the the magnetometers are significantly closer to the magnetic sources than they are to the proof masses for the linear approximation to be efficient. In fact, numerical experiment shows that were the sources farther away the results would correspondingly improve.

2.3 Numerical simulations

In order to have a more quantitative idea of the actual performance of the above interpolation scheme, a somewhat simplified model of the physical situation was implemented and analysed. The model has the following ingredients and assumptions:

---

[4] Note that the field is proportional to $\boldsymbol{\nabla}[r^l\,Y_{lm}(\mathbf{n})]$, which is a first degree polynomial in this case.

	DDS-LTP	**Ref.**	S2-IEC-TN-3052
IEEC		**Version**	1.0
	Neural Network algorithms for	**Date**	11-Mar-2009
	magnetic diagnostics in the LTP	**Page**	13/20

1. The sources of magnetic field in the LCA are point dipoles outside the LCA.

2. According to that, the magnetic field created by the dipole distribution at a generic point $\mathbf{x}$ and time t is given by

$$\mathbf{B}(\mathbf{x}, t) = \frac{\mu_0}{4\pi} \sum_{a=1}^{n} \frac{3\left[\mathbf{m}_a(t) \cdot \mathbf{n}_a\right] \mathbf{n}_a - \mathbf{m}_a(t)}{\left|\mathbf{x} - \mathbf{x}_a\right|^3} \qquad (2.15)$$

where $\mathbf{n}_a = (\mathbf{x} - \mathbf{x}_a)/|\mathbf{x} - \mathbf{x}_a|$ are unit vectors connecting the the a-th dipole $\mathbf{m}_a$ with the field point $\mathbf{x}$, and n is the number of dipoles.

3. The sources correspond to a set identified by ASU. Their positions in the S/C are known, and so are the moduli of their dipole moments. The set itself as well as the source parameters needs to be updated, but the sample used (which dates back to November 2006) is good enough for the pursued objectives.

4. Fluctuations of the dipoles, both in modulus and direction, are unknown, but DC values suffice to check the numerical performance of the algorithms described in section 2.2.

As already mentioned, this model can be refined, but is sufficient at this stage. The idea behind it is to compare interpolated magnetic field results with exact ones in a number of realistic mission circumstances. By this the following is meant:

- A fixed number of magnetic dipoles, 37 in this case, is assumed. Each dipole has its own fixed position in space, and a fixed modulus.

- The *orientations* of the dipoles are unknown, instead. An interpolation example is thus characterised by a specific selection of the 37 source dipole orientations.

- In order to explore the algorithm behaviour, a batch of examples are examined, each one corresponding to a randomly generated set of dipole orientations.

The most salient features of the anlysis can be briefly summarised:

1. Magnetic field estimation errors are very variable, ranging from exultant $\sim 2\%$ to apalling $\sim 2000\%$.

2. These enormous variances happen in an utterly random and fully unpredictable way.

Figure 2.3 shows the statisitics of a batch of 1000 algorithm runs. Variances are not reflected in the plots, but the average errors incurred are already indicative of the clear inadequacy of the interpolation method.

The conclusion is thus quite simple: the intrinsic linear character of the interpolation scheme is not capable of reproducing the field map structure inside te LCA —hence in the TMs—, and therefore can produce very good or very bad results *by accident*. Neither is predictable, the *average* error being too high anyway.
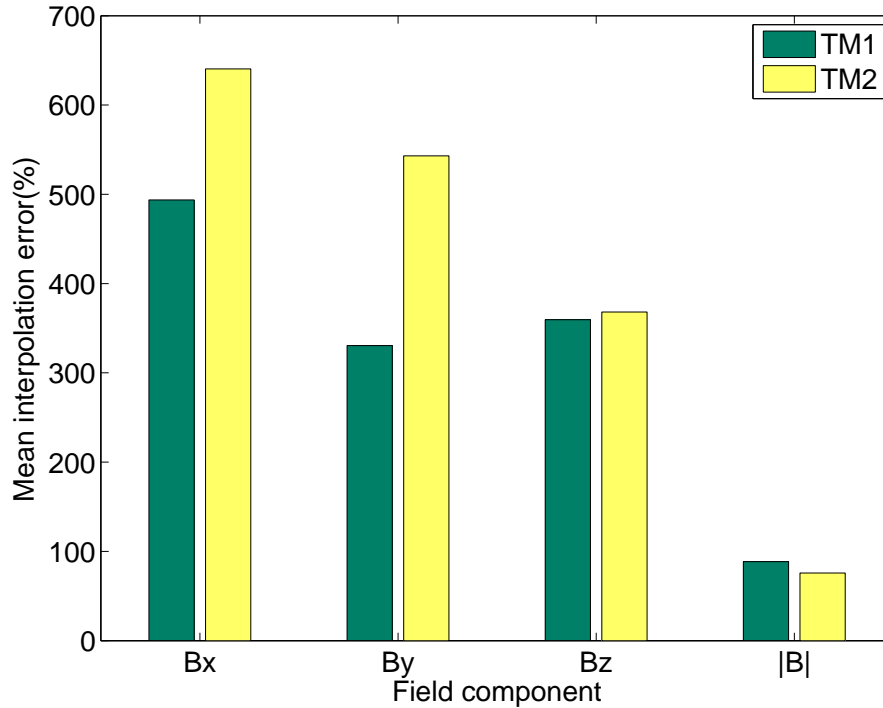
Figure 2.3: Averaged estimation errors in the components of the magnetic and of its modulus. They are reported in relative percent, i.e., $100(\text{real} - \text{estimated value})/(\text{real value})$. Colors correspond to each of the LTP TMs, respectively.

2.4 A more contrived interpolation scheme

An attempt to improve the situation was also implemented by means of a different approach: this consists in estimating the magnetic field inside the LCA by means of a *weighted average* of the magnetometers readouts:

$$\mathbf{B}_{\text{weighted}}(\mathbf{x}) = \sum_{s=1}^{4} a_s(\mathbf{x}) \mathbf{B}(\mathbf{x}_s) \tag{2.16}$$

where the weights $a_s(\mathbf{x})$ are of the form

$$a_s(\mathbf{x}) = \frac{|\mathbf{x} - \mathbf{x}_s|^{\alpha}}{\sum_{p=1}^{4} |\mathbf{x} - \mathbf{x}_p|^{\alpha}} \tag{2.17}$$

i.e., proportional to the α-th power of the distance between the field point and the specified magnetometer. Some numerical experiments have shown that a value $\alpha = -1/2$ produces close to optimum results for the field at the TMs, but the errors incurred are very similar in practice to the ones reported in the previous section. Again, this seems not to be on the right track for a solution to the problem.

	DDS-LTP	**Ref.**	S2-IEC-TN-3052
IEEC		**Version**	1.0
	Neural Network algorithms for	**Date**	11-Mar-2009
	magnetic diagnostics in the LTP	**Page**	15/20

3 A novel approach: Neural Networks

Search of an alternative approach to the above interpolation schemes is imperative, otherwise the information provided by the magnetometers will hardly be useful for the main goal of the LTP magnetic diagnostics, i.e., to quantify the contribution of the magnetic noise to the total system noise. Here some promising preliminary results are presented on the implementation of a completely different methodology: *Neural Networks*.

Artificial neural networks are made up of interconnecting artificial neurons (programming constructs that mimic the properties of biological neurons) that have the property of *learning* from processing data. Neural networks are often used in solving nonlinear classification and regression tasks by learning from data, hence are worth trying with the present problem.

There are four sets of tasks which need to be implemented when solving a problem with artificial neural networks:

1. Neuron model
2. Model and architecture
3. Learning paradigm and learning algorithm
4. Performance assessment

3.1 Neuron model

The *neuron* is the basic unit of any neural network. It performs the following two operations —see figure 3.1:

- It collects the inputs from all other neurons connected to it and computes a weighted sum of the signals the latter inject into it, generally adding a *bias* as well. If we represent the inputs by a vector $\mathbf{x} \equiv (x_1, \ldots, x_n)$, and the weights by a $\mathbf{w} \equiv (x_1, \ldots, w_n)$ then this operation consists in calculating the sum

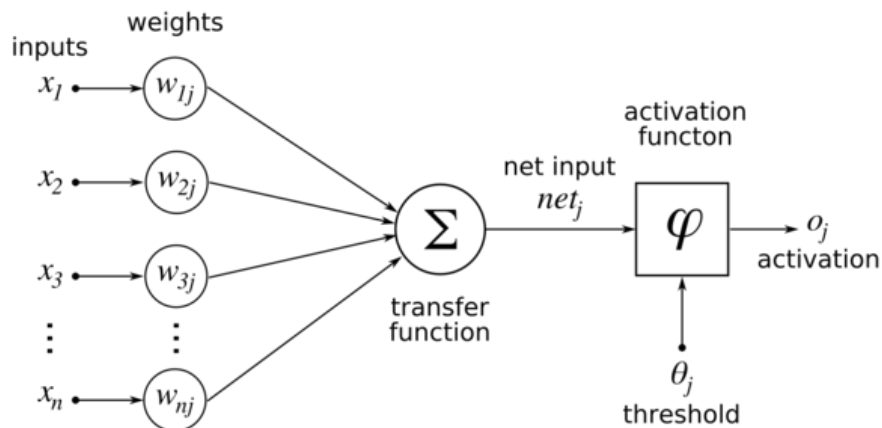$$\Sigma = w_0 + \sum_{k=1}^{n} w_k x_k = w_0 + \mathbf{w}^T \mathbf{x} \tag{3.1}$$

Figure 3.1: Schematics of the operations performed by an artificial neuron.

where the superindex T stands for transpose matrix; in this case, $\mathbf{w}^T$ is a row vector while $\mathbf{x}$ is a column vector, so that $\mathbf{w}^T\mathbf{x}$ is the scalar product of $\mathbf{w}$ and $\mathbf{x}$. Finally, w_0 is the bias.

- The above sum is used as the argument to the so called *activation function*, $\varphi(\Sigma)$. The neuron's output, also known as its *activation*, is thus

$$o = \varphi(\Sigma) \tag{3.2}$$

In general, $\varphi(\Sigma)$ can be selected in many different ways; here, differentiable activation functions will be used, which suit well the gradient descent back-propagation learning algorithm —see section 3.3 below.

3.2 Neural network architecture

Artificial neural networks are software or hardware models inspired by the structure and behaviour of biological systems, and they are created by a set of neurons distributed in layers. There are many different types of neural networks in use today, but the architecture of a so called *feed-forward network*, where each layer of neurons is linked with the next by means of a set of weights, is the most commonly used, and will also be used here.

In this preliminary study, the above architecture has been adopted, see figure 3.2: magnetometers' data streams will be considered the system inputs, while magnetic field results and their gradients at the positions of the test masses will be the system outputs.
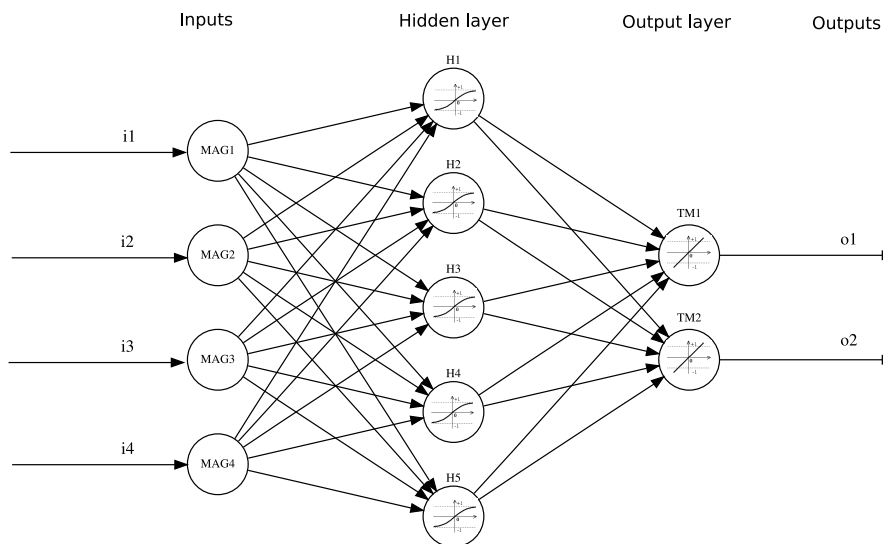

Figure 3.2: Feed-forward neural network architecture. Magnetometers readings are the system inputs, and estimates of the field and gradient at the positions of the test masses are the outputs of the system. In this architecture, one only intermediate, or *hidden* layer is assumed. Each of the circles represents one neuron and corresponds to the model shown in figure 3.1.

	DDS-LTP	**Ref.**	S2-IEC-TN-3052
IEEC	Neural Network algorithms for	**Version**	1.0
	magnetic diagnostics in the LTP	**Date**	11-Mar-2009
		Page	17/20

3.3 Learning paradigms and learning/training algorithms

The investigation of learning algorithms is currently an active field of research. The design and implementation of an adequate training scheme is the essential ingredient for a good quality estimation of the magnetic field and its gradient at the LTP TMs.

3.3.1 Learning paradigms

There are two major learning paradigms, each corresponding to a particular abstract learning task. These are *supervised learning* and *unsupervised learning.*

1. **Supervised learning.** The idea of this is quite clearly suggested by its very name: a set of *examples* is filed, which consists in a number of vector of inputs (magnetometers' readouts in this case) and the corresponding values of the magnetic field and its gradient at the TMs for a given (chosen) distribution of dipoles in the S/C. Let x represent a generic input vector, and y the associated vector output. These two vectors constitute an example. The set of filed examples for supervised learning is thus a set of pairs (x, y), where $x \in X$ and $y \in Y$, X and Y being some suitable sample spaces.

   The network is then fed the inputs x of one example and let it work out an output, o, say. This output is then compared with the correct one, y, and an error is calculated if $o \neq y$. Iterations are then triggered to adjust the weighting factors such that the error is minimised. These will however vary as different examples are run, so a *cost function* is defined which enables the network to optimise the set of weights which works best for the set of examples analysed, based on some given criterion.

2. **Unsupervised learning.** In unsupervised learning a cost function is to be minimised as well, but this function can be any relationship between x and the network output, o. The cost function is determined by the task formulation. Unsupervised learning is thus a form of self-adaptive system, whose guide is not an *a priori* knowledge of the final result but knowledge gained from experience.

In either case, the learning process is based on the architecture of the network, i.e., number of neurons and layers and their interconnections, as well as on the activation functions. These are parameters which, at least in the simplest cases, are tuned *ab initio* by the user based on observed performance of the network.

In this study, supervised learning has been the implemented learning paradigm. Analysis has been done with the help of the *Matlab* software suite.

3.3.2 Learning algorithms

There are many algorithms for training neural networks. When training feed-forward neural networks with supervised learning, a back-propagation algorithm is usually implemented. The error of the mapping at the output is propagated backwards in order to readjust the weights and improve the output error for the next iteration.

The propagation can be implemented with different methods, the *Ideal Gradient Descent* being a classic which will also be used here. The method is widely used in the field of soft computing, and is a variant of the method of steepest descent.

	DDS-LTP	**Ref.**	S2-IEC-TN-3052
IEEC		**Version**	1.0
	Neural Network algorithms for	**Date**	11-Mar-2009
	magnetic diagnostics in the LTP	**Page**	18/20

Iterations on the weights of the different neurons at the different layers proceed according to the following algorithm:

$$\mathbf{w}_{n+1} = \mathbf{w}_n - \eta \left. \frac{\partial E}{\partial \mathbf{w}} \right|_n \tag{3.3}$$

where n labels the current iteration step, and η is the learning rate, adjustable by the user. E is the sum over the set of training examples of the square errors of the outputs:

$$E = \sum_{\text{examples}} (\mathbf{o} - \mathbf{y})^T (\mathbf{o} - \mathbf{y}) \tag{3.4}$$

where $\mathbf{o}$ is the (vector) output from the network, while $\mathbf{y}$ is the *target*, or correct output in the corresponding example. This E can only be defined in supervised learning, of course, and the idea of the above procedure is to find that point in weight space where E is the minimum possible. E can therefore be considered the cost function to be minimised in this particular supervised training scheme, also known as *batch mode* as the analysis is done across the entire set of training patterns in a single block.

There are a number of technical issues in pursuing the iterations in equation (3.3), such as the choice of the initial set of weights, identification of local minima of E, boundary effects, etc. which need to be addressed in each specific case. We skip any detailed discussion of these matters here.

3.4 Performance assessment

In this last step, the trained network must be tested with examples which differ from those used in the learning process. This is needed to assess whether or not the trained neural network is able to generate the expected results when fed with previously unseen inputs, hence determine its usability for the specific purpose it is intended.

4 Results

This section reviews the results obtained so far —preliminary. Training and testing have been done based on different field realisations, using information provided by ASU on 37 magnetic dipole sources within the spacecraft.

Two different batches of examples, each including 1 000 realisations of a possible magnetic environment, have been generated following the directives in the bulletted list of page 13. The first batch has been used as the training set for a neural network with 12 inputs (3 inputs for each of the 4 vector magnetometers) and 6 outputs representing the field information at the position of the 2 test masses (3 field components for each test mass). The second batch has been used for validation to assess the performance of the net in front of unseen magnetometers readings.

As a further extension, another network has been trained, including the magnetic field gradient values in the output vector.
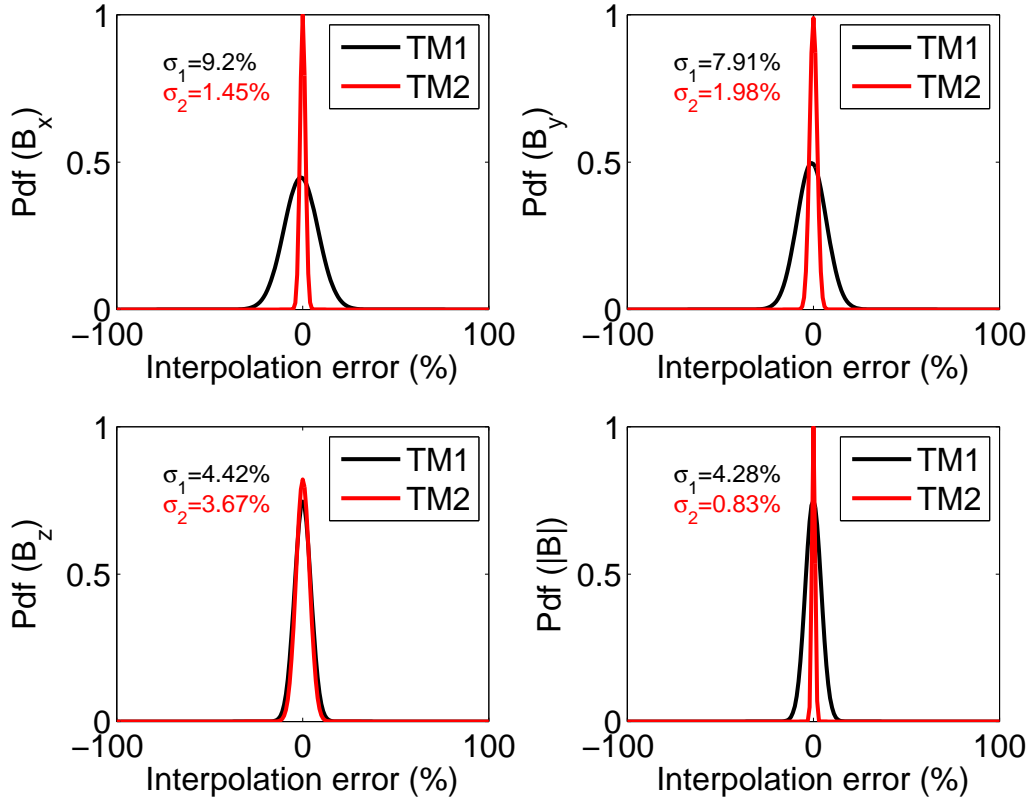
Figure 4.1: Probability density function of the error distributions for each field component at the position of test mass 1 (black trace) and test mass 2 (red): top left plot for B_x, top right for B_y, bottom left for B_z and bottom right for $|\mathbf{B}|$.

4.1 Field estimation results

Figure 4.1 shows the probability density functions of the errors in the estimates of the components of the magnetic field at the positions of each TMs. The plot is based on the outcome of the 1 000 validation runs described in the previous section. Units are percentage errors. As can be observed, the order of magnitude of the errors of the estimated fields are now within much more acceptable margins (around 10-15%). This improvement represents the reduction of estimation errors by more than one order of magnitude in comparison with the former methods.

4.2 Field gradient estimation results

The magnetic field gradient can and should also be estimated. An extension of the network has accordingly been developed to estimate it at the TMs. The 9 components $\partial B_i / \partial B_j$ of the gradient are not independent, since they must verify equations (2.2) which reduces their number to 5. Neural network estimates of the gradient components does not guarantee that those conditions are verified, but this is not a problem, as discrepancies are within tolerance errors. Neural network approaches can also generate other similar inconsistencies with rigorous analytic results but, again, these can be dealt with.

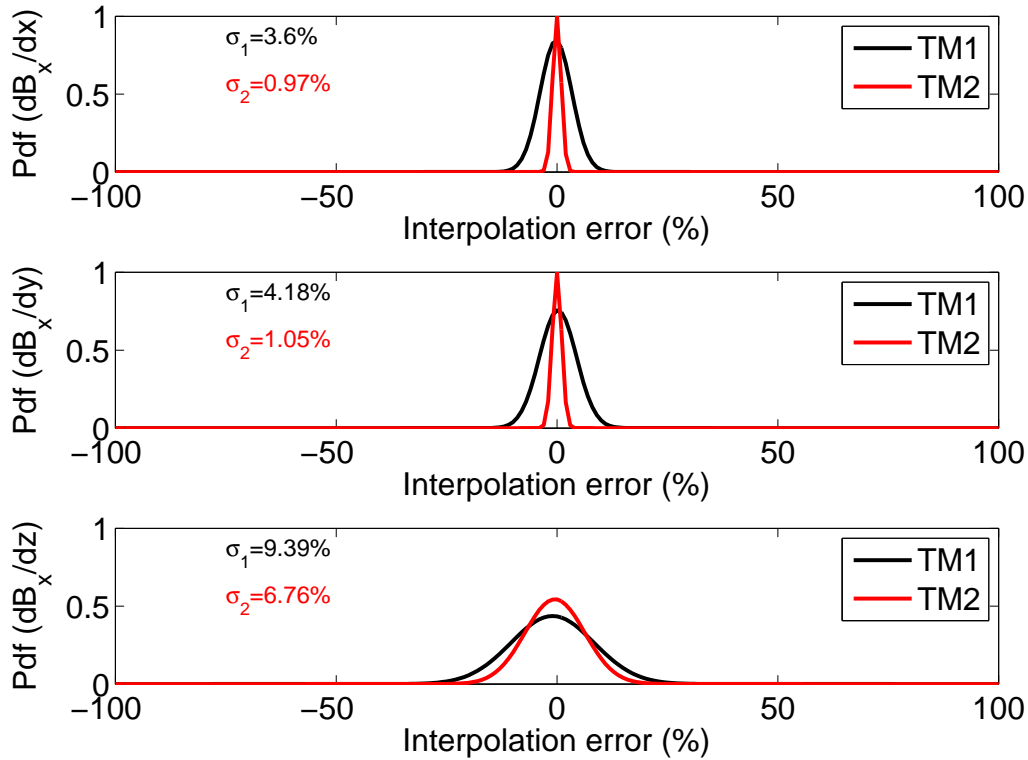A first batch of results on gradient estimation is shown in figure 4.2 for $\boldsymbol{\nabla} B_x$ and at the

	DDS-LTP	**Ref.** S2-IEC-TN-3052
IEEC	Neural Network algorithms for	**Version** 1.0
	magnetic diagnostics in the LTP	**Date** 11-Mar-2009
		Page 20/20

Figure 4.2: Probability density function of the errors distribution for the three components of $\boldsymbol{\nabla} B_x$. From top to bottom: $\partial B_x/\partial x$, $\partial B_x/\partial y$ and $\partial B_x/\partial z$ at the positions of the test masses. Errors are given in percents, black traces corresponding to TM1, and red ones to TM2.

positions of both TMs. As may be observed, they are also within much more acceptable margins than the earlier interpolation approach could produce.

5 Conclusion

The magnetic diagnostic sensor set in the LTP is such that to infer the magnetic field and gradient on the TMs based on their readouts is far from simple. More or less conventional interpolation schemes cannot generally go beyond the linear approximation, which grossly fails to produce reliable results, so *Artificial Neural Network* models are under investigation. The preliminary results reported herein are encouraging, as the network learning process is able to significantly improve estimation errors.

The main problem is the adequacy of a training process to the set of data the magnetometers will deliver in flight. This underlines the need to characterise on ground to our best ability the magnetic properties of the S/C and LCA at all locations and working conditions, both regarding their DC and fluctuating values. Reliable information on that appears to be essential for a meaningful assessment of magnetic noise in the LTP.